


Fungal transformation of selenium and tellurium located in a volcanogenic sulfide deposit

Xinjin Liang,^{1†} Magali Aude Marie-Jeanne Perez,²
Shuai Zhang,^{3‡} Wenjuan Song,^{1,4}
Joseph Graham Armstrong,⁵ Liam Adam Bullock,^{5§}
Jörg Feldmann,² John Parnell,⁵ Laszlo Csetenyi⁶ and
Geoffrey Michael Gadd ^{1,7*}

¹Geomicrobiology Group, School of Life Sciences,
University of Dundee, Dundee DD1 5EH, Scotland, UK.

²Trace Element Speciation Laboratory (TESLA),
Department of Chemistry, King's College, Meston Walk,
University of Aberdeen, Aberdeen AB24 3UE,
Scotland, UK.

³School of Science and Engineering, University of
Dundee, Dundee DD1 4HN, Scotland, UK.

⁴Xinjiang Institute of Ecology and Geography, Chinese
Academy of Sciences, Urumqi, 830011, China.

⁵Department of Geology and Petroleum Geology, King's
College, Meston Walk, University of Aberdeen, AB24
3UE, Aberdeen, Scotland, UK.

⁶Concrete Technology Group, Department of Civil
Engineering, University of Dundee, Dundee,
Scotland, UK.

⁷State Key Laboratory of Heavy Oil Processing, Beijing
Key Laboratory of Oil and Gas Pollution Control, College
of Chemical Engineering and Environment, China
University of Petroleum, 18 Fuxue Road, Changping
District, 18 Fuxue Road, Changping District, Beijing,
102249, China.

Summary

Microbial reduction of soluble selenium (Se) or tellurium (Te) species results in immobilization as elemental forms and this process has been employed in soil bioremediation. However, little is known of direct and indirect fungal interactions with Se/Te-bearing ores. In this research, the ability of *Phoma glomerata* to

effect transformation of selenite and tellurite was investigated including interaction with Se and Te present in sulfide ores from the Kisgruva Proterozoic volcanogenic deposit. *Phoma glomerata* could precipitate elemental Se and Te as nanoparticles, intracellularly and extracellularly, when grown with selenite or tellurite. The nanoparticles possessed various surface capping molecules, with formation being influenced by extracellular polymeric substances. The presence of sulfide ore also affected the production of exopolysaccharide and protein. Although differences were undetectable in gross Se and Te ore levels before and after fungal interaction using X-ray fluorescence, laser ablation inductively coupled plasma mass spectrometry of polished flat ore surfaces revealed that *P. glomerata* could effect changes in Se/Te distribution and concentration indicating Se/Te enrichment in the biomass. These findings provide further understanding of fungal roles in metalloid transformations and are relevant to the geomicrobiology of environmental metalloid cycling as well as informing applied approaches for Se and Te immobilization, biorecovery or bioremediation.

Introduction

Selenium (Se) and tellurium (Te) species can be transformed through oxidation, reduction, methylation and demethylation by microorganisms (Gadd, 1993; Jacob *et al.*, 2016; Eswayah *et al.*, 2016). Such processes are important components of natural biogeochemical cycles for these elements in natural aquatic and terrestrial environments as well as those polluted with potentially toxic levels (Gadd, 1993, 2007, 2010; Rosenfeld *et al.*, 2017). Reduction and methylation in particular have been employed successfully for bioremediation of Se-contaminated waters and sediments through immobilization and volatilization respectively (e.g. Lawson and Macy, 1995; Cantafio *et al.*, 1996; Brady *et al.*, 1996; Soda *et al.*, 2012; Mal *et al.*, 2017; Piacenza *et al.*, 2018a,b). In recent years, with growing concern

Received 20 February, 2020; accepted 1 April, 2020. *For correspondence. E-mail g.m.gadd@dundee.ac.uk; Tel. (+44) 1382 384767. †Present addresses: Sustainable Environment Research Centre, Upper Glyntaff, University of South Wales, Pontypridd, Wales, CF37 4BD, UK; ‡School of Mechanical and Aerospace Engineering, Queen's University, Belfast, BT9 5AG, UK; §Ocean and Earth Science, University of Southampton, National Oceanography Centre, Southampton, SO14 3ZH, UK.

about the security of supply of strategic elements for electronic, digital and environmentally sustainable (bio) technologies, microbial processes are viewed as an important part of the suite of approaches that may be necessary for element biorecovery (Nancharai et al., 2016; Liang and Gadd, 2017). The application of microbial Se or Te oxyanion reduction offers a potential route for biorecovery of these elements since extensive extracellular precipitation of elemental Se or Te can occur in solution (Gharieb et al., 1999; Baesman et al., 2007; Espinosa-Ortiz et al., 2017; Liang et al., 2019). However, little is known about direct fungal interactions with Se- or Te-containing mineral deposits, and their applied or environmental significance, particularly in the solid phase.

The ores at the massive Kisgruva Proterozoic volcanogenic sulfide deposit in the Kongsberg region of Buskerud, Norway, were originally used for extraction of copper, iron and sulfur. However, they also contain high concentrations of Se and Te (Bjerkgård, 2015; Bullock et al., 2018; Kotková et al., 2018). The Se and Te in these ores are primarily retained in pyrite and chalcopyrite as selenides and tellurides with selenite and tellurite occurring at ore surfaces as oxidized weathering products (Bullock et al., 2018). Little is known about fungal interactions with Se and Te species present in ores and their ability to effect changes in chemical state or mobility, although it is known that fungi can have significant effects on ores and substrates containing other metals. For example, the wood-rotting basidiomycete *Schizophyllum commune* can bioweather black slate through hyphal mechanical pressure and biochemical mechanisms such as siderophore, laccase and organic acid excretion (Kirtzel et al., 2020). *Aspergillus niger* can mediate direct and indirect bioleaching of cobalt from low grade laterite and pyritic ores (Yang et al., 2019, 2020). Fungal bioweathering, involving both mineral dissolution and biomineralization mechanisms, has also been demonstrated for silicate and sulfide ores (Wei et al., 2012a, 2013), manganese oxides including birnessite (Wei et al., 2012b), mimetite (Ceci et al., 2015a), and vanadinite (Ceci et al., 2015b). Investigation of fungal interactions with Kisgruva sulfide ore can provide understanding of how heterogeneously distributed critical elements, like Se and Te, may be transformed or accumulated by fungi. This may be significant for environmental metalloid cycling as well as novel approaches for Se and Te immobilization, bioremediation or biorecovery. Therefore, this research has examined the capability of *Phoma glomerata* as a selenite- and/or tellurite-reducing microorganism and further examined its potential to interact with and accumulate Se and Te from samples from the Kisgruva volcanogenic sulfide deposit. Specific objectives were to characterize extracellular and intracellular

deposition of Se and Te nanoparticles, including the role of extracellular polymeric substances, effects of Se/Te oxyanions on growth and morphology, and fungal accumulation of Se and Te from resources present in the sulfide ores.

Results and discussion

Effects of selenite and tellurite on growth and morphology of P. glomerata

In order to examine the effects of Se and Te oxyanions on growth and morphology, 1 mM sodium selenite or sodium tellurite was incorporated in AP1 liquid media and growth of *P. glomerata* recorded after 30 days. Control *P. glomerata* hyphae showed a typical appearance and smooth surface texture (Fig. 1Aa), whereas hyphae grown with selenite (Fig. 1Ba) or tellurite (Fig. 1Ca) appeared thinner with a shrunken appearance and a loose surface texture (Fig. 1). The subcellular architecture of *P. glomerata* was investigated using a confocal microscope after addition of Hoechst 33342 which reveals nuclear distribution. Control mycelium possessed elongated nuclei (Fig. 1Ac), while the addition of selenite and tellurite increased septation in the hyphae (Fig. 1Bc and Cc), and swelling was observed from the hyphal tip with addition of tellurite (Fig. 1Cc). The nuclear density on addition of selenite and tellurite was increased compared to controls. These observations complement other research on the effect of different Se levels on growth of *Pleurotus eryngii* (Kim et al., 2014). A biomass reduction and increased septation also occurred when *P. eryngii* was grown at 1 mM Se (Kim et al., 2014). It has also been found that selenite was capable of binding to polysaccharides and was particularly linked to chitin in the cell wall of *Pleurotus ostreatus* (Munoz et al., 2006). Low concentrations of selenite can stimulate fungal growth reflecting its importance as an essential element (Munoz et al., 2006; Kim et al., 2014).

Formation of elemental Se and Te during growth of P. glomerata

Nanoparticles formed on fungal surfaces and in the medium during growth of *P. glomerata* with selenite/tellurite. Spherical Se-containing particles occurred in fungal supernatants after growth with selenite (Fig. 2A), while needle-shaped particles (nanorods) formed after growth with tellurite (Fig. 2B). The Te nanorods harvested from *P. glomerata* culture supernatants clustered together being composed of numerous individual shards (Fig. 2B). Particle size analysis revealed that the particles formed after fungal growth with Na₂SeO₃ or Na₂TeO₃ showed significant variability. The average diameter of

Se-containing particles ranged from 100 to 200 nm, with a high proportion of sizes less than 140 nm (Fig. 2C). The particle size (width) of tellurite-containing particles ranged from 10 to 80 nm, with a high proportion of sizes less than 40 nm (Fig. 2D). The particle size measurements provide an average diameter for spherical shapes,

but are not so applicable for the Te nanorods where width measurements were used.

Energy-dispersive X-ray analysis (EDXA) was used to elucidate the elemental composition of the particles produced by *P. glomerata*. Most particles generated after growth with 1 mM Na_2SeO_3 showed peaks for carbon, oxygen and Se as the main elements (Fig. 2E). Similarly, particles generated after fungal growth in AP1 medium amended with 1 mM Na_2TeO_3 showed peaks for carbon, oxygen and Te as the main elements (Fig. 2F). XRD data showed that the Se-containing particles produced by *P. glomerata* showed a match to reference patterns for elemental Se (Se), while the Te-containing particles produced by *P. glomerata* matched elemental Te (Te) (Fig. 3). The formation of spherical-shaped elemental Se and needle-shaped elemental Te particles conforms to previously published findings (Mandal *et al.*, 2006; Baesman *et al.*, 2007; Bajaj *et al.*, 2012; Aborode *et al.*, 2015; Borghese *et al.*, 2016; Rosenfeld *et al.*, 2017; Espinosa-Ortiz *et al.*, 2015a,b, 2016a,b,c, 2017). Reduction of selenite and tellurite to elemental Se and Te can occur intracellularly (Gharieb and Gadd, 1998, 2004; Gharieb *et al.*, 1999; Debieux *et al.*, 2011; Sonkusre *et al.*, 2014; Li *et al.*, 2014; Espinosa-Ortiz *et al.*, 2017) and/or extracellularly (Oremland *et al.*, 2004; Baesman *et al.*, 2007; Zhang *et al.*, 2012; Jiang *et al.*, 2012; Bajaj *et al.*, 2012; Vetchinkina *et al.*, 2013; Borghese *et al.*, 2016) among different microorganisms. In this study, it appeared that elemental Se and Te formed both intracellularly, as shown in the DIC images (Fig. 1Bb and Cb), and extracellularly. Extracellular production of elemental Se and Te resulted in particles that could reach sizes of

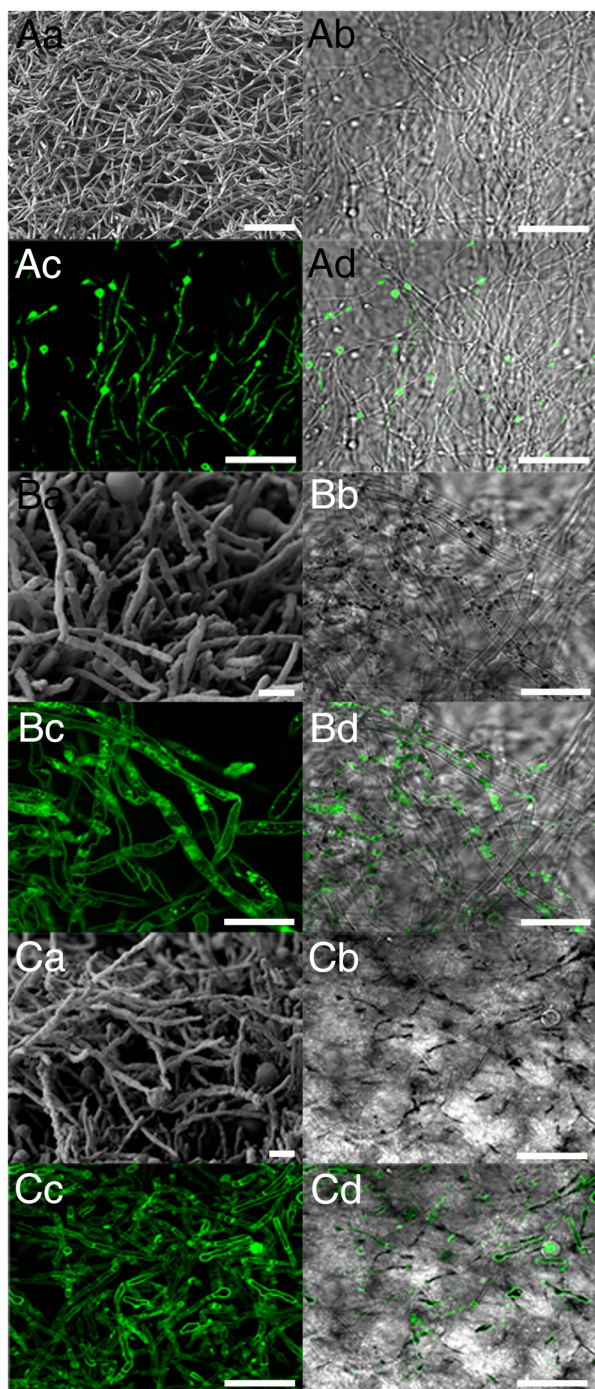


Fig. 1. SEM, differential interference contrast (DIC) imaging and confocal microscopy (CM) of *P. glomerata* grown in AP1 liquid media amended with 1 mM Na_2SeO_3 or Na_2TeO_3 .

A. *P. glomerata* grown in AP1 medium as the control, (Aa) SEM of *P. glomerata* mycelium, (Ab) DIC image of *P. glomerata* mycelium, (Ac) CM of *P. glomerata* nuclear distribution after Hoechst 33342 staining, (Ad) superimposed images of DIC and Hoechst 33342 staining. Scale bars: Aa 10 μm , Ab-d 50 μm .

B. *P. glomerata* grown in AP1 medium amended with 1 mM Na_2SeO_3 , (Ba) SEM of *P. glomerata* mycelium grown with Na_2SeO_3 , (Bb) DIC image of *P. glomerata* mycelium grown with Na_2SeO_3 , (Bc) CM of nuclear distribution of *P. glomerata* grown with Na_2SeO_3 after Hoechst 33342 staining, (Bd) superimposed images of DIC and Hoechst 33342 staining of *P. glomerata* grown with Na_2SeO_3 . Scale bars: Ba 10 μm , Bb-d 20 μm .

C. *P. glomerata* grown in AP1 medium amended with 1 mM Na_2TeO_3 , (Ca) SEM of *P. glomerata* mycelium grown with Na_2TeO_3 , (Cb) DIC image of *P. glomerata* mycelium grown with Na_2TeO_3 , (Cc) CM of nuclear distribution of *P. glomerata* grown with Na_2TeO_3 after Hoechst 33342 staining, (Cd) superimposed images of DIC and Hoechst 33342 staining of *P. glomerata* grown with Na_2TeO_3 . Scale bars: Ca 10 μm , Cb-d 50 μm . *Phoma glomerata*, with or without selenite and tellurite, was grown for 30 days at 25°C in the dark on an orbital shaking incubator at 125 rpm. Typical images are shown from one of at least three examinations.

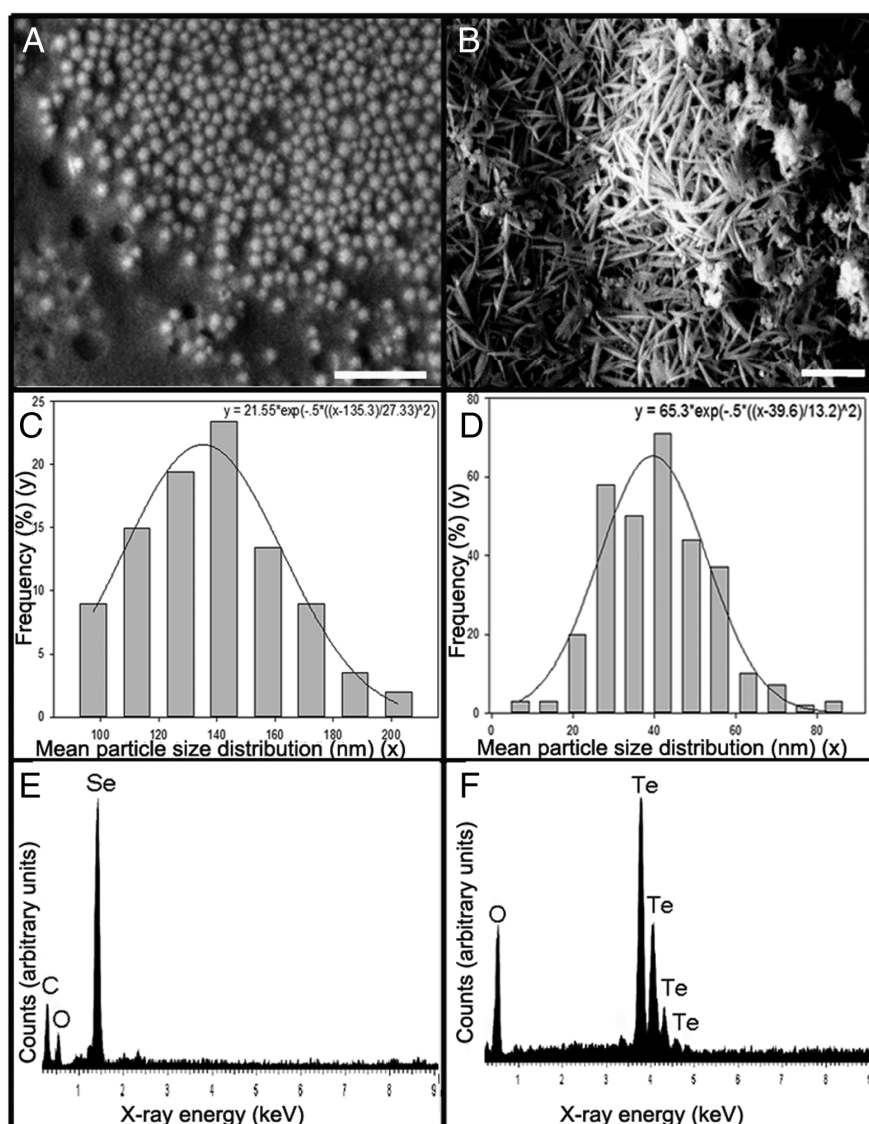


Fig. 2. SEM, PSD and energy dispersive X-ray analysis of nanoparticles harvested from spent culture medium supernatants after growth of *P. glomerata* with 1 mM Na_2SeO_3 or Na_2TeO_3 . Nanoparticles harvested from the supernatant of *P. glomerata* grown in (A) Na_2SeO_3 - or (B) Na_2TeO_3 -amended AP1 medium. Scale bars: A = 1 μm, B = 500 nm. Size distribution of particles generated from *P. glomerata* growth with (C) Na_2SeO_3 or (D) Na_2TeO_3 . (E) Se- or (F) tellurium-containing particles produced by *P. glomerata* (shown in A, B). *Phoma glomerata* was grown in AP1 liquid media amended with 1 mM Na_2SeO_3 or Na_2TeO_3 for 30 days at 25°C in the dark on an orbital shaking incubator at 125 rpm. Typical images, measurements and spectra are shown from one of at least three examinations.

around 140 nm (Se^0) (Fig. 2C) and 80 nm (Te^0) as mentioned previously (Fig. 2D). From our observations, it seemed the majority of biogenic Se and Te nanoparticles were generated extracellularly.

The influence of selenite or tellurite on fluorescent components of EPS

Excitation emission matrix (EEM) fluorescence spectra of the extracellular polymeric substance (EPS) produced by *P. glomerata* grown without (Fig. 4A) or with 1 mM Na_2SeO_3 (Fig. 4B) or 1 mM Na_2TeO_3 (Fig. 4C) are shown in Fig. 4. Three excitation peaks were identified for the EPS extracted from *P. glomerata* grown without selenite or tellurite: peak A 2700 (Ex/Em 370/460 nm), peak B 395.2 (Ex/Em 290/360 nm) and peak C

848 (Ex/Em 270/465 nm). These peaks correspond to humic acid-like substances (peak A), tryptophan and protein-like soluble microbial by-products (peak B), and fulvic acid-like and humic acid-like substances (peak C) (Chen *et al.*, 2003). Only one excitation peak was found for the EPS extracted from *P. glomerata* grown with selenite or tellurite: peak 2308 (Ex/Em 370/455 nm) for selenite and peak 1455 (Ex/Em 375/456 nm) for tellurite, both being classed as indicating humic acid-like substances (Chen *et al.*, 2003). Previous research has demonstrated that exopolysaccharide from *Lactococcus lactis* was able to react with Se chloride oxide and generate Se-exopolysaccharide (Se-EPS) (Guo *et al.*, 2013). Gold nanoparticles (AuNPs) were formed and aggregated at pH 2 in a cell-free extract of *Avena sativa* (Armendariz *et al.*, 2004). The formation of these aggregates was due

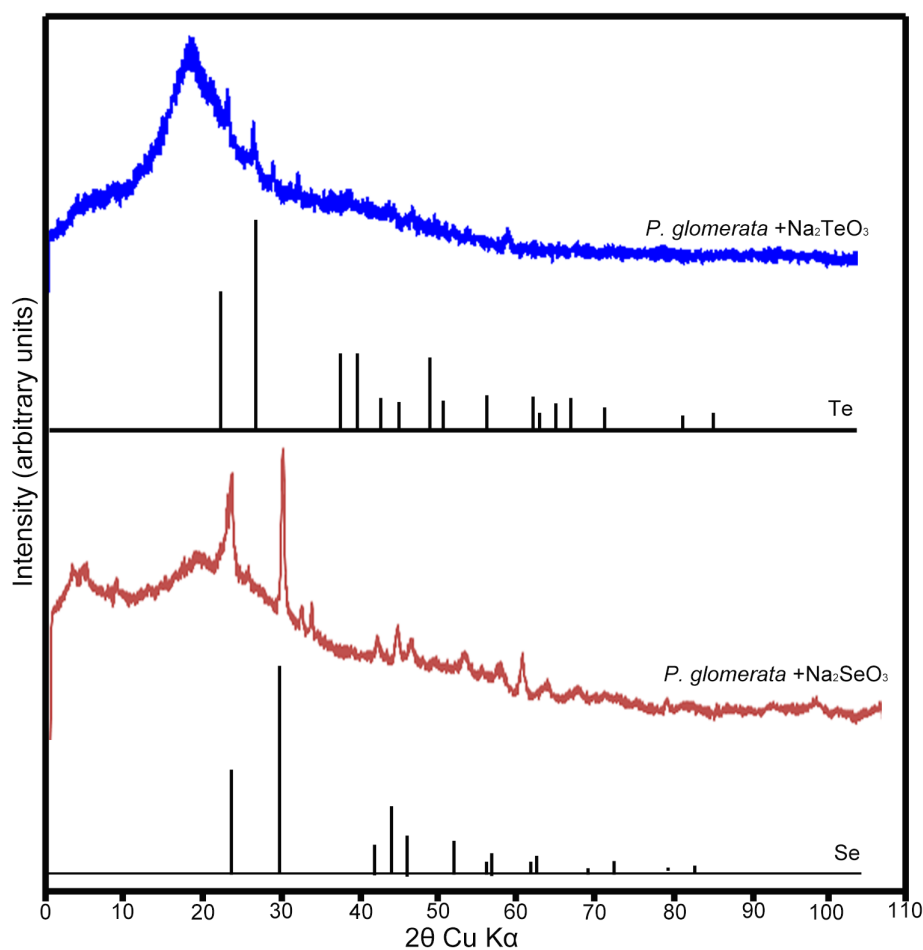


Fig. 3. X-ray powder diffraction patterns of particles formed in 1 mM Na_2SeO_3 - or Na_2TeO_3 -amended AP1 liquid medium after growth of *P. glomerata* at 25°C in the dark at 125 rpm for 30 days. Patterns for dominant components and diffraction patterns of particles produced because of *P. glomerata* activity are shown. (Se), elemental Se; (Te), elemental tellurium. Typical diffraction patterns are shown from one of several determinations.

to protonation caused by the accessibility of carboxyl groups with a pK_a below pH 3 and demonstrated the role of EPS in formation of the metal nanoparticles (Armendariz *et al.*, 2004). Several proteins and

associated EPS from several bacterial strains have been shown to play a role in the generation and stability of various metal nanoparticles, including AuNPs, silver nanoparticles (AgNPs), cadmium nanoparticles

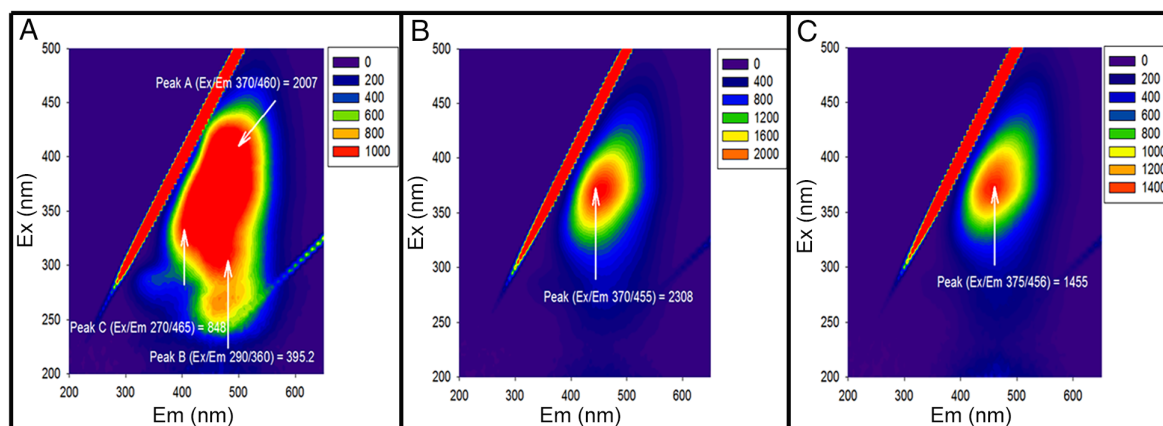


Fig. 4. EEM fluorescence spectra of (A) soluble EPS and (B) Se- or (C) tellurium-bound EPS obtained from *P. glomerata* culture medium. *Phoma glomerata* was grown in AP1 liquid media amended with 1 mM Na_2SeO_3 or Na_2TeO_3 for 30 days at 25°C in the dark on an orbital shaking incubator at 125 rpm. Colour intensities are in arbitrary units, and typical spectra are shown from one of at least three examinations with typical relative standard deviations of about 5%.

(CdSNPs), Se nanoparticles (SeNPs), and Te nanoparticles (TeNPs) (Ahmad, *et al.*, 2003; Sweeney *et al.*, 2004; Birla *et al.*, 2009; Aborode *et al.*, 2015; Jain *et al.*, 2015; Borghese *et al.*, 2016). EPS can govern the surface charge of Se nanoparticles and also their size and shape (Jain *et al.*, 2015). Functional groups characteristic of proteins and carbohydrates from EPS can stabilize spherical Se nanoparticles maintaining their shape and colloidal properties (Jain *et al.*, 2015). Similar findings have been observed for biotransformation of tellurite to elemental Te with a loosely bound EPS fraction (Mal *et al.*, 2017).

Fourier transform infrared and thermogravimetric/differential thermal analysis of elemental Se and Te formed by P. glomerata

Fourier transform infrared (FTIR) spectroscopy can measure the wavelength and intensity of the absorption of infrared (IR) radiation by samples. The vibrations of a structural repeat unit can be used to identify different polypeptides and proteins from the IR spectral data. There are nine characteristic IR absorption bands, which are amide A, amide B, and amide I–VII. The most significant vibrational bands of a protein backbone usually fall in the amide I and amide II bands. C=O stretch vibrations account for about 80% of the peptide linkages, which usually indicate protein secondary structural components in the amide I band ($1700\text{--}1600\text{ cm}^{-1}$). The amide II band usually illustrates in-plane NH bending and CN stretching (Kong and Yu, 2007). Details of the characteristic IR bands of peptide linkages and vibration modes can be found in the study by Banker (1992). FTIR spectra of the purified Se and Te nanoparticles generated by *P. glomerata* indicated the presence of various capping biomolecules on the nanoparticle surfaces (Fig. 5A and C). These are substances produced as a result of biotic activity, e.g. proteins and amino acids, which can associate with nanoparticles and affect their properties including size (Jain *et al.*, 2015; Mal *et al.*, 2017; Li and Gadd, 2017; Piacenza *et al.*, 2018a,b; Liang *et al.*, 2019; Liu *et al.*, 2019). The wave numbers of the maxima for the main bands revealed in the FTIR spectra are labelled in Fig. 5A and C. The typical protein bands were attributable to amide I at 1637.76 cm^{-1} for SeNPs (Fig. 5A) and 1637.15 cm^{-1} for TeNPs (Fig. 5C), some low-intensity amide II at 1454.58 cm^{-1} (symmetrical stretching vibrations of —COO—), and amide III at 1336.90 cm^{-1} were detected for SeNPs (Fig. 5A). These observations match other results for Se nanoparticles synthesized by *Azospirillum thiophilum* and *Alternaria alternata* (Sarkar *et al.*, 2011; Tugarova *et al.*, 2017). The typical polysaccharide vibration regions are usually detected within the range of $1000\text{--}1200\text{ cm}^{-1}$. Polysaccharide peaks at

1084.79 cm^{-1} and 1045.11 cm^{-1} were detected for SeNPs (Fig. 5A) while peaks at 1081.82 cm^{-1} were found for TeNPs (Fig. 5C). These peaks were attributable to aromatic in-plane C—H bending (Sharma *et al.*, 2014). The strong broad peak at $3000\text{--}3500\text{ cm}^{-1}$ could be attributed to the amine N—H stretching vibration and occurred at 3303.51 cm^{-1} for SeNPs (Fig. 5A) and at 3303.84 cm^{-1} for TeNPs (Fig. 5C) (Krimm and Bandekar, 1986; Sarkar *et al.*, 2011; Sharma *et al.*, 2014). Even after several purification steps (see Methods), these results clearly demonstrated the strong attachment of proteins and polysaccharides as capping biomacromolecules on the SeNPs and TeNPs. These data are in line with the EEM results (Fig. 4) and other relevant findings for biosynthesised Se nanoparticles (Sarkar *et al.*, 2011; Sharma *et al.*, 2014; Tugarova *et al.*, 2017).

Thermogravimetric analysis (TGA), derivative thermogravimetry (DTG), and differential thermal analysis (DTA) were carried out for the Se-/Te-containing particles formed by *P. glomerata*. The TG/DTA thermogram is shown in Fig. 5B and D. For elemental Se formed by *P. glomerata* (Fig. 5B), the initial total weight loss of 4.86% observed at temperatures up to 150°C is attributable to the removal of adsorbed moisture and some organic volatiles, which are also associated with the derivative peak A as shown in Fig. 5B. Between 150°C and 230°C , the total weight loss was 23.57%, which may be related to low-molecular weight organic substances (LMWOSs). Between 150°C and 230°C , the total weight loss was 58.5%, which resulted from the decomposition of fungal biomass and extract derivatives, which is associated with the derivative peak C as shown in Fig. 5B. Similar thermogravimetric observations have been observed for Se-containing derivatives synthesized from *Cordyceps militaris* polysaccharide (Zhu *et al.*, 2016). Similar results were obtained from the elemental Te formed by *P. glomerata* (Fig. 5D). The FTIR and TGA results illustrate the association of extracellular protein and exopolysaccharide with the nanoparticles, and their role in stabilizing the size and shapes of Se and Te nanoparticles can be inferred and supported by previous research (Jain *et al.*, 2015; Mal *et al.*, 2017; Piacenza *et al.*, 2018a,b; Liang *et al.*, 2019).

As suggested from the above results, the formation of elemental Se and Te, confirmed by XRD analysis, occurred both intracellularly and extracellularly, as has been found for many other bacteria and fungi. There are several mechanisms involved in the formation of biogenic Se and Te nanoparticles, such as those mediated by intracellular proteins and extracellular EPS. It was previously shown that the formation of biogenic Se and Te nanoparticles was strongly influenced by the presence of EPS, which can be a complex mixture of extracellular proteins, lipids, extracellular DNA, humic substances,

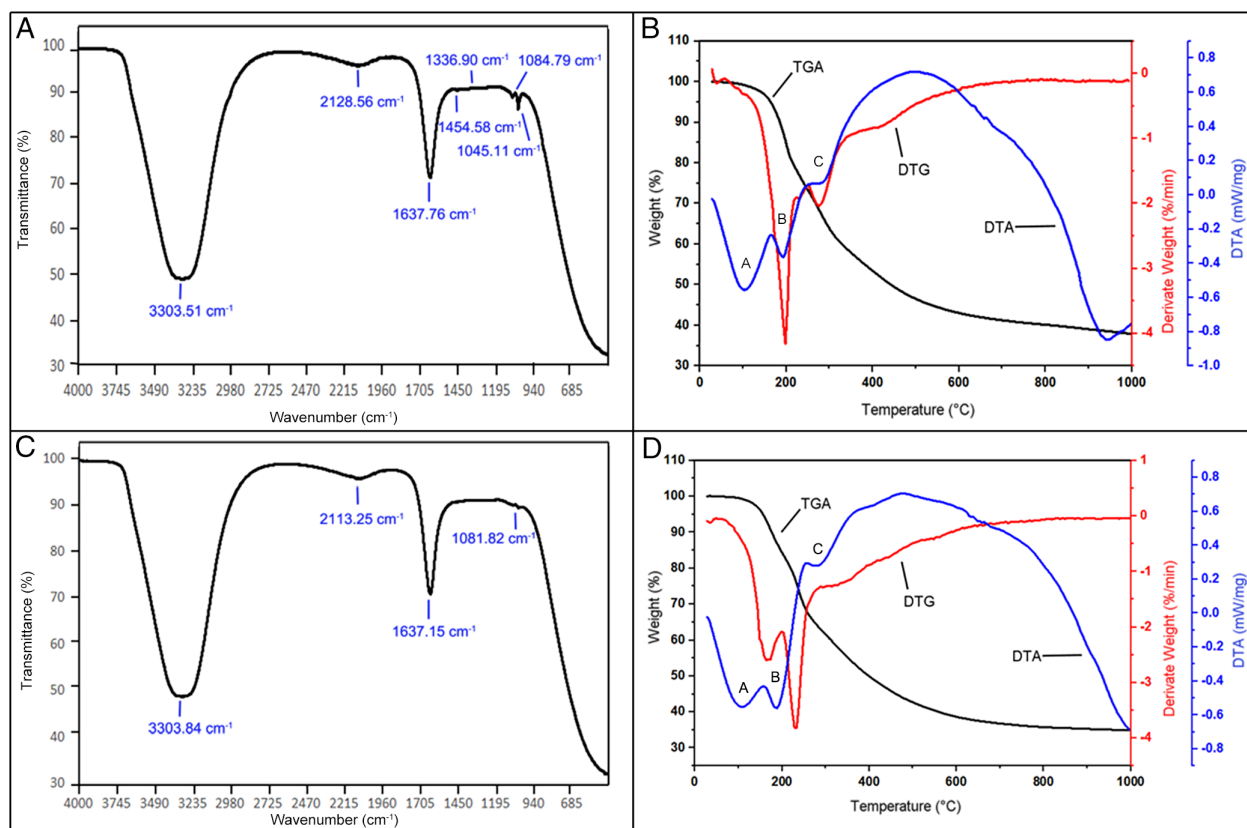


Fig. 5. Fourier transform infrared spectra and thermogravimetric analysis (TGA) of SeNPs (A, C) and TeNPs (B, D) generated by *P. glomerata*. *Phoma glomerata* was grown in AP1 liquid media amended with 1 mM Na₂SeO₃ or Na₂TeO₃ for 30 days at 25°C in the dark on an orbital shaking incubator at 125 rpm. Typical spectra are shown from one of at least three examinations with typical relative standard deviations of about 5%. DTG, derivative thermogravimetry; DTA, differential thermal analysis.

and polysaccharides providing a multiplicity of functional groups (Sarkar *et al.*, 2011; Sharma *et al.*, 2014; Tugarova *et al.*, 2017; Piacenza *et al.*, 2018a,b). Several researchers have previously demonstrated a role for EPS and protein in capping elemental Se and Te produced by fungi and their roles in particle stabilization and the prevention of aggregation (Jain *et al.*, 2015; Mal *et al.*, 2017; Piacenza *et al.*, 2018a,b).

Distribution and concentration of Se and Te in Kisgruva sulfide ores

Sequential extraction and speciation were performed on Kisgruva sulfide ores 450 and 459 to determine total concentrations of Se and Te species adsorbed onto oxide minerals and bound to organic matter (Bullock *et al.* 2018). Amounts of Se and Te species adsorbed to charged surfaces were determined by a phosphate buffer extraction method (Fig. 6, blue), while the amounts and speciation of Se and Te adsorbed to organic matter were examined by a sodium hydroxide extraction method (Fig. 6, orange). The Aqua regia residues method was

used for total concentrations of Se and Te (Fig. 6, grey). Both selenite (SeO₃²⁻) and tellurite (TeO₃²⁻) were identified in sulfide ore crust samples by the extraction methods used (Fig. 6), but elemental forms (Se⁰ and Te⁰) or selenate (SeO₄²⁻)/tellurate (TeO₄²⁻) were not detected. For sample 450, the proportions of Se and Te species adsorbed to charged surfaces of, e.g. oxide minerals were 5.66% and 6.89%, the proportions of Se and Te species associated with organic matter were 8.67% and 24.49%, and the proportions of Se and Te bound to non-extractable matter were 85.67% and 70.90% respectively. Of the extractable Se (14.3% of the total Se), only 39.5% remained with oxide minerals, with 60.5% being bound to organic matter [Se(-II)]. For extracted Te (31.4% of the total Te), 22% was adsorbed to oxide minerals, and 78% bound to organic matter. Similar results were observed for sample 459, where the proportions of Se and Te species adsorbed to oxide minerals were 5.63% and 4.43%, the proportions of Se and Te adsorbed to organic matter were 21.35% and 19.74%, and the proportions of Se and Te adsorbed to non-extractable matter were 73.03% and 77.27%

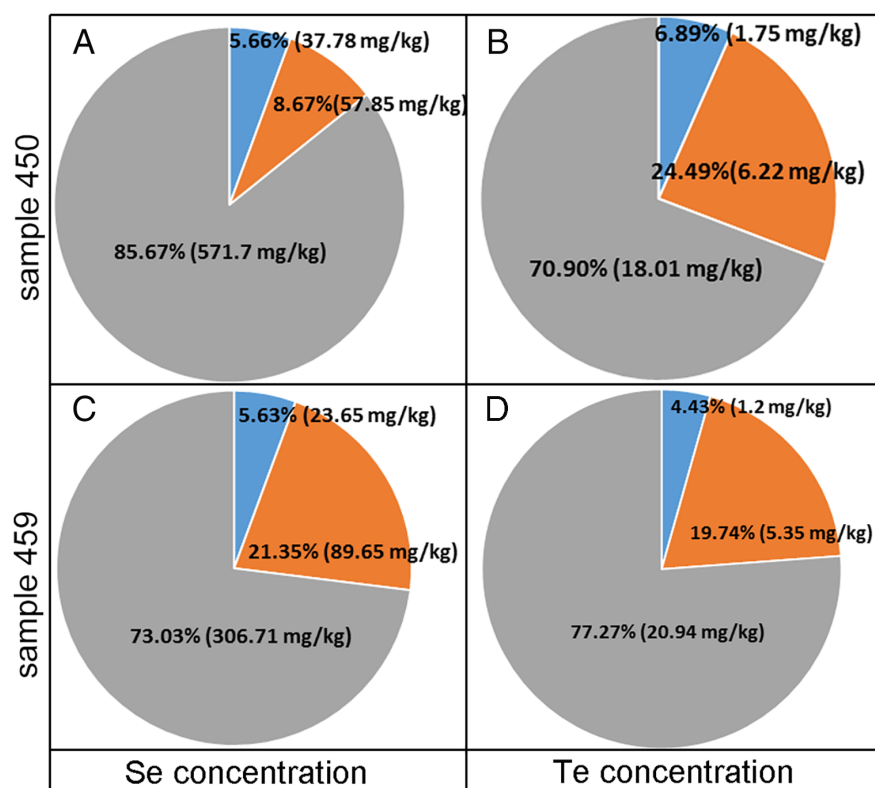


Fig. 6. Se and Te speciation determined by phosphate buffer (blue), sodium hydroxide (orange) and aqua regia residues (grey) extraction methods for ore samples 450 and 459. (■) Concentrations of Se or Te on charged surfaces, such as oxides or clay minerals, assessed through phosphate buffer extraction. (■) Concentrations of Se or Te bound to organic matter assessed through NaOH extraction. (■) Total extractable Se or Te assessed through aqua regia residues extraction after the previous sequential extraction procedures. All values shown are means of at least three measurements with typical relative standard deviations of about 5%.

respectively. Of the extractable Se (27% of total Se), only 20.94% remained with oxide minerals, with 79.10% bound to organic matter (Se(-II)). For extracted Te (24.2% of total Te), 20.94% was adsorbed to oxide minerals, and 79.10% bound to organic matter (Fig. 6).

pH changes and tolerance, polysaccharide and protein production in sulfide ore amended liquid media

Phoma glomerata could grow in the presence of 1% Kisgruva sulfide ores 450 or 459 over a 30 days incubation period. When ores 450 and 459 were suspended in sterile Milli-Q water, the suspension pH values were pH 3.9 and 7.9 respectively. There were significant changes in medium pH values on addition of the sulfide ore samples compared to the control. The initial medium pH for *P. glomerata* grown in ore-free AP1 medium was

pH 6.3. Compared to the control, the addition of sample 450 lowered the pH from pH 6.3 to pH 2.6 and remained acidic. Sample 459 increased the pH from pH 6.3 to pH 8.3 and remained alkaline (Table 1). Tolerance indices (TIs) were used to compare biomass yields grown in AP1 medium with or without the sulfide ore samples (Table 1). A TI value lower than 100% indicated growth inhibition. *Phoma glomerata* was able to grow in the presence of sulfide ores 450 and 459 for 30 days at 25°C. However, *P. glomerata* showed a 70.6% and 64.6% reduction of growth in the presence of samples 450 and 459 respectively. The altered pH was likely to be contributing to this inhibition as well as any toxic effects arising from the ore samples.

The presence of Kisgruva sulfide ore also had an effect on exopolysaccharide production by *P. glomerata*. The concentration of exopolysaccharide produced by

Table 1. The pH, polysaccharide and total protein content of fungal culture supernatant, and TI, after growth of *P. glomerata* in liquid AP1 medium for 30 days at 25°C in the dark in the presence or absence of Kisgruva ore samples 450 and 459. All measurements are means of at least three replicates with typical relative standard deviations of about 5%.

	pH	TI (%)	Polysaccharide content (mg l ⁻¹)	Protein content (mg l ⁻¹)
Control	6.3	100.0	25.8 ± 0.6	102.8 ± 1.3
Sample 450	2.6	70.6	11.7 ± 0.3	34.9 ± 0.9
Sample 459	8.3	64.6	7.5 ± 0.5	51.3 ± 0.7

Table 2. Elemental composition (% by mass) of Kisgruva sulfide ore samples 450 and 459 before and after growth of *P. glomerata* in liquid medium for 30 days at 25°C in the dark, as determined using XRF. Most elements are expressed as oxides.

Element	Initial composition sample 450	Composition after fungal growth sample 450	Initial composition sample 459	Composition after fungal growth sample 459
Sum	100%	100%	100%	100%
Fe ₂ O ₃	30.44	31.65	28.07	31.52
SO ₃	39.93	39.76	30.66	28.93
SiO ₂	9.71	7.08	19.88	17.85
P ₂ O ₅	1.69	5.78	0.089	0.81
Al ₂ O ₃	8.43	5.36	11.98	10.19
MgO	4.92	3.45	6.29	5.24
K ₂ O	0.32	0.94	1.06	2.46
Cu	1.75	2.15	0.24	0.29
TiO ₂	0.16	0.17	0.40	0.35
Cl	0.14	0.62	0.01	0.87
Zn	2.10	2.51	0.51	0.65
Na ₂ O	0	0	0.29	0.05
Se	0.04	0.06	0.02	0.02
CaO	0.15	0.20	0.24	0.49
MnO	0.09	0.09	0.19	0.19
As	0.02	0.02	0.02	0.02
Pb	0.04	0.05	0.01	0.01
Co	0.02	0.02	0.04	0.04
W	0.06	0.07	0.01	0.02

Data shown are average values from at least three measurements with typical relative standard deviations of about 5%.

P. glomerata grown in control ore-free liquid AP1 medium was 25.8 mg l⁻¹ (Table 1). The exopolysaccharide concentration from *P. glomerata* grown with sample 450 in AP1 medium was reduced to 11.7 mg l⁻¹, with a greater reduction being observed for sample 459 (7.5 mg l⁻¹) (Table 1). Extracellular protein production correlated with the pattern of exopolysaccharide production. Compared to the control, the amount of extracellular protein decreased after growth with the Kisgruva sulfide ore samples. Control *P. glomerata* grown in AP1 medium produced extracellular protein at around 102.8 mg l⁻¹ (Table 1). In the presence of samples 450 and 459, the protein concentrations dropped to 34.9 mg l⁻¹ and 51.3 mg l⁻¹ respectively (Table 1). Such reductions largely reflected the inhibitory effects of the ores on growth of *P. glomerata*.

Composition of sulfide ore before and after fungal growth

Elements present in the sulfide ore samples were determined by X-ray fluorescence (XRF). Se and Te were present within the sulfide ores in pyrite and chalcopyrite (samples 450 and 459), which contained up to 688 ppm Se and 81 ppm Te (Bullock *et al.*, 2018). There were no significant differences observed in the composition of the sulfide ores 450 and 459 before and after fungal growth, probably because any changes in elemental composition mediated by the fungus were small in relation to total element concentration (Table 2).

Fungal accumulation of Se and Te from sulfide ore

Phoma glomerata was used for further experiments on Se and Te accumulation when interacting with the sulfide ores. *Phoma glomerata* was grown on polished flat surfaces of samples 450 and 459 for 30 days on malt extract agar. About 50 cm³ malt extract agar (MEA, LabM Ltd, Bury, Lancashire, UK) (autoclaved at 121°C, 15 min) were cooled to a temperature of around 50°C prior to pouring in 180 mm diameter Petri dishes. Samples 450 and 459, pre-sterilized by oven-drying at 105°C to constant weight, were placed centrally in the Petri dishes with the polished flat surface facing upwards. Dialysis membranes (Focus Packaging and Design, Louth, UK) were sterilized by autoclaving twice at 121°C for 15 min in Milli-Q water, and used to cover the agar with or without the ore sample. These served to separate the fungus from the medium, but still allow access to diffusible nutrients, and enable easy removal of the biomass. Inocula consisted of a 10 mm diameter core cut from the margins of an actively growing fungal colony placed in the centre of the membrane disc. Plates were sealed with parafilm and incubated at 25°C in the dark for the duration of the experiments. Control and sample-amended plates for each experiment were made from the same batch of MEA powder. After 30 days incubation, fungal biomass on samples 450 and 459 was removed and laser ablation mapping was carried out on the sample surfaces. Laser ablation maps showed Se and Te to a low extent before fungal growth, even though Se was generally high throughout the pyrite phase (Figs. 7C and 8C). For Se

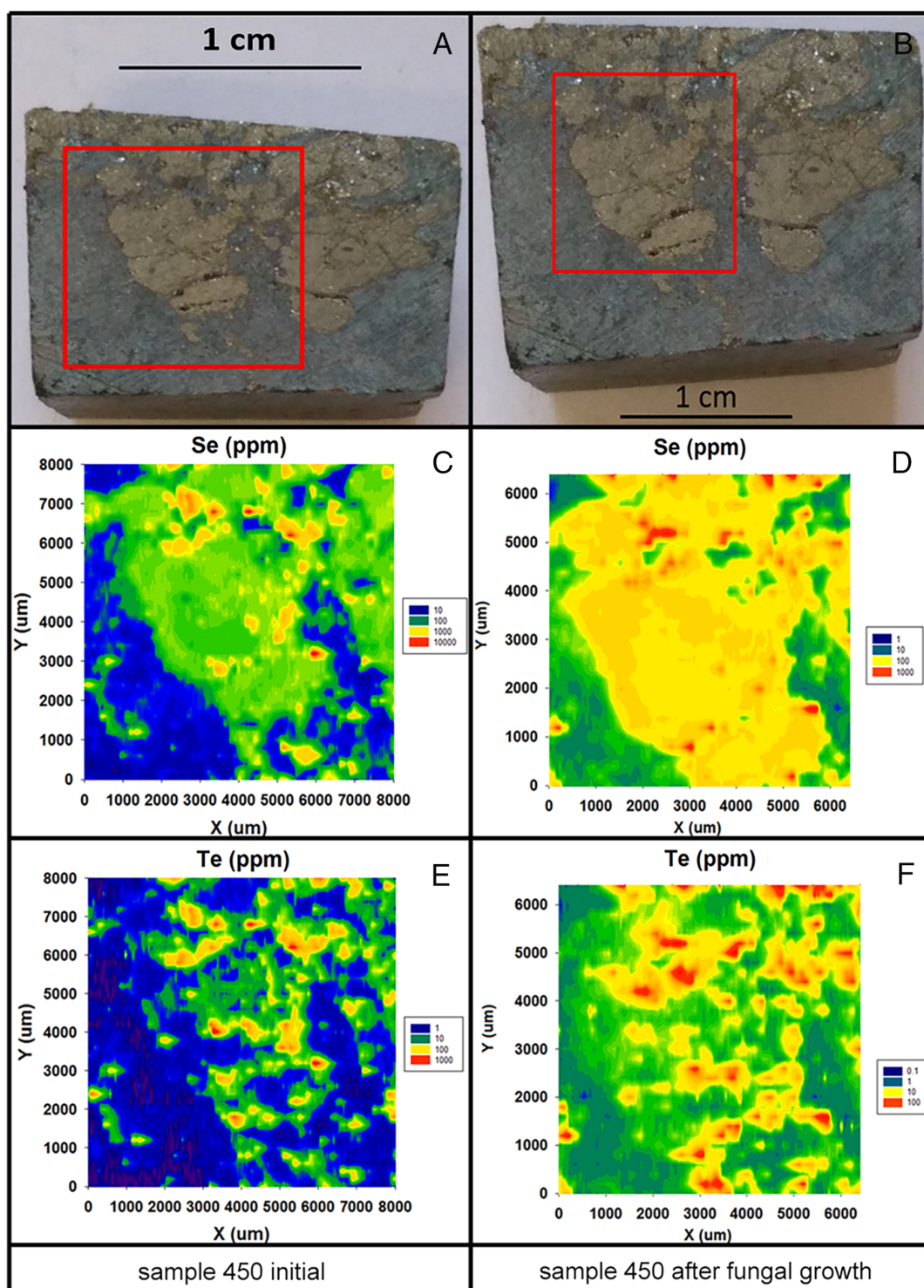


Fig. 7. Laser ablation inductively-coupled plasma mass spectrometry (LA-ICP-MS) elemental maps of Se and Te distribution on predominantly inclusion-free pyrite phases from Kisgruva sulfide ore sample 450 before and after being grown with *P. glomerata* for 30 days at 25°C in the dark. Scale bar = 1 cm. Typical spectra are shown from one of at least three determinations.

and Te, concentrations were highest towards the edges of the pyrite for samples 450 and 459 (Figs. 7C, E and 8C, E). As well as a high content throughout pyrite, Se

and Te also showed localized areas of high concentration, in some instances up to 10 000 ppm and 1000 ppm respectively (Figs. 7 and 8). Although the selected pyrite

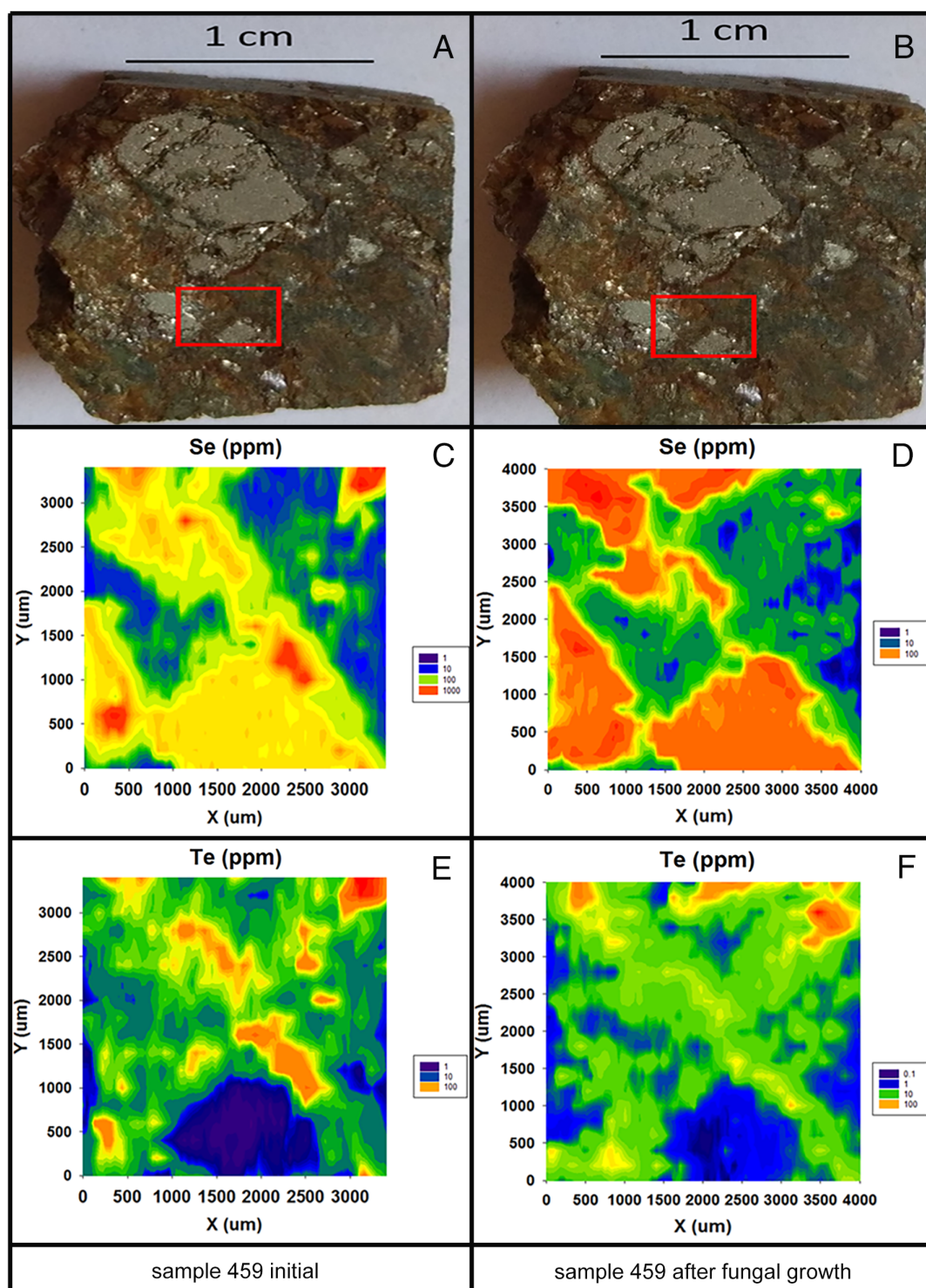


Fig. 8. Laser ablation inductively coupled plasma mass spectrometry (LA-ICP-MS) element maps of Se and Te distribution on predominantly inclusion-free pyrite phases from Kisgruva sulfide ore sample 459 before and after being grown with *P. glomerata* for 30 days at 25°C in the dark. Scale bar = 1 cm. Typical spectra are shown from one of at least three determinations.

crystals were generally inclusion-free, these Se and Te hotspots may correspond to micron-sized Se^{2-} and Te^{2-} deposits (Bullock *et al.*, 2018). After growth with

P. glomerata, Se and Te hotspot concentrations for sample 450 dropped to 1000 ppm and 100 ppm respectively (Fig. 7), while for sample 459, concentrations decreased

Table 3. Concentrations of all elements in Kisgruva sulfide ore samples 450 and 459 before and after growth with *P. glomerata* for 30 days at 25°C in the dark. Data shown are average values from at least three measurements with typical relative standard deviations of about 5%.

Element (ppm)	Sample 450			Sample 459		
	Before	After	EF	Before	After	EF ¹
Fe	390 041	169 915	1.00	633 668	216 849	1.00
Cu	476	256	1.23	2124	402	0.55
As	408	168	0.95	376	137	1.06
Se	645	218	0.78	688	158	0.67
Ag	26	14	1.24	62	15	0.71
Te	49	14	0.66	81	23	0.83
Au	0.2	0.1	1.15	0.2	0.1	1.46
Hg	0.7	0.4	1.31	1.4	1.3	2.71
Pb	1274	471	0.85	189	125	1.93
Bi	17	5	0.68	30	9	0.88

EF indicates the enrichment factor that is expressed relative to the iron in the ore samples, before and after fungal growth. An EF value <1 indicates an elemental decrease.

to 100 ppm for both Se and Te (Fig. 8). These results correspond with Se and Te removal from the ores and enrichment in the fungus after growth of *P. glomerata* (Table 3).

Samples 450 and 459 were high in other chalcophilic elements, which show a chemical affinity to Se and Te, such as Fe (380 041 ppm, 633 668 ppm), Cu (476 ppm, 2124 ppm), As (408 ppm, 376 ppm), Ag (26 ppm, 62 ppm) and Bi (17 ppm, 30 ppm) respectively. The sulfide ore samples contained an average of 0.05% total organic carbon (TOC) (data not shown). Using laser ablation ICP-MS analysis of polished ore surfaces, it was found that certain elements in the sulfide ore samples showed a reduction after growth with *P. glomerata*, as revealed by the enrichment factors (expressed relative to the iron concentration before and after fungal growth). An EF value <1 indicate an elemental decrease, and therefore removal and enrichment in the fungal biomass, and this was clear for Se and Te with EF values ranging from 0.66 to 0.83 (Table 3). As mentioned previously, changes in Se and Te localization in the sulfide ores were confirmed by LA-ICP-MS element mapping (Figs. 7 and 8). Together, these results demonstrate that *P. glomerata* can accumulate metal(oids) from the sulfide ores.

The interactions of microorganisms with metalliferous ores have been studied for many years, being relevant to understanding the geomicrobiology of elemental cycling and mineral transformations in the environment as well as for industrial exploitation. The ability of certain bacteria and archaea to extract metals from ores and concentrates is well known and the basis of commercial metal bioleaching (Schippers *et al.*, 2013; Johnson *et al.*, 2013; Johnson, 2014). Fungi are also capable of metal bioleaching from ores, with secreted organic acids being a key component of the process (Burgstaller and Schinner, 1993; Mehta *et al.*, 2010; Anjum *et al.*, 2010; Biswas *et al.*, 2013; Schippers *et al.*, 2013; Yang *et al.*, 2019,

2020). However, fungal bioleaching has not been demonstrated for Se or Te species, the most important Se transformations being reduction or methylation (Gadd, 1993; Chasteen and Bentley, 2003; Rosenfeld *et al.*, 2017). The production of elemental Se/Te species results in Se/Te immobilization and has been investigated in the context of element biorecovery from solution, and soil and water bioremediation by prokaryotes and fungi (Lawson and Macy, 1995; Cantafio *et al.*, 1996; Soda *et al.*, 2012; Espinosa-Ortiz *et al.*, 2015b, 2016b; Eswayah *et al.*, 2016; Nancharaiiah *et al.*, 2016; Rosenfeld *et al.*, 2017; Liang and Gadd, 2017). In this work, we have demonstrated the capability of a model fungus *P. glomerata* to mediate Se and Te transformations, resulting in Se or Te nanoparticle formation, and the involvement of biomacromolecules (proteins and polysaccharides) in this process. We have also shown that this organism can directly interact with a Se-/Te-containing sulfide ore sample causing changes in metalloid speciation and accompanied by accumulation of the metalloids by the fungus and removal from the substrate. Fungal activity is therefore resulting in element fractionation, redistribution and concentration. To our knowledge, this is the first demonstration of such a phenomenon in a mineral ore and adds further understanding of fungal roles in metalloid geomicrobiology and environmental cycling.

Experimental procedures

Organism, media and culture conditions

Phoma glomerata ([Corda] Wollenw. and Hochapfel) from the Geomicrobiology Group culture collection was used for experiments. Previous work has already demonstrated its ability for iron oxide nanoparticle and nano-silver formation (Birla *et al.*, 2009; Gudadhe *et al.*, 2011;

Gade *et al.*, 2014). *Phoma glomerata* was routinely maintained on malt extract agar (MEA) (Sigma-Aldrich, St. Louis, MO, USA) at 25°C in the dark, and AP1 medium (composition detailed below) was used for experiments in liquid medium. Sodium selenite (Na_2SeO_3) (Sigma-Aldrich) or sodium tellurite (Na_2TeO_3) (Alfa Aesar, Lancashire, UK) were used at a 1 mM final concentration to examine the effect of these Se or Te oxyanions on growth.

The 100 ml of AP1 liquid cultures of *P. glomerata* in 250-ml Erlenmeyer conical flasks were maintained on an orbital shaking incubator (Infors Multitron Standard, Ritttergasse, Switzerland) at 125 rpm at 25°C in the dark. For the liquid cultures, *P. glomerata* was grown for 5 days on AP1 agar medium after which 10 × 6 mm diameter inoculum plugs were taken from the margins of actively growing colonies using sterile cork borers (autoclaved at 121°C, 15 min) and inoculated into AP1 liquid medium. AP1 liquid medium consists of (L^{-1} Milli-Q water) (Merck Millipore, Billerica, MA, USA): D-glucose 30 g (Merck, Readington Township, NJ, USA), $(\text{NH}_4)_2\text{SO}_4$ 5 g (Sigma-Aldrich), KH_2PO_4 0.5 g (Sigma-Aldrich), $\text{MgSO}_4 \cdot 7\text{H}_2\text{O}$ 0.2 g (VWR, Radnor, PA, USA), $\text{CaCl}_2 \cdot 6\text{H}_2\text{O}$ 0.05 g (VWR), NaCl 0.1 g (Sigma-Aldrich), $\text{FeCl}_3 \cdot 6\text{H}_2\text{O}$ 2.5 mg (Sigma-Aldrich), and trace metals: $\text{ZnSO}_4 \cdot 7\text{H}_2\text{O}$ 4 mg (VWR), $\text{MnSO}_4 \cdot 4\text{H}_2\text{O}$ 4 mg (VWR), and $\text{CuSO}_4 \cdot 5\text{H}_2\text{O}$ 0.4 mg (VWR). All chemicals, apart from glucose, were prepared as 1 M stock solutions and autoclaved separately (121°C, 15 min) before appropriately combining the required volumes to reach the desired final concentrations for AP1 liquid medium. Sodium selenite (Na_2SeO_3) or sodium tellurite (Na_2TeO_3) stock solution (1 M) in Milli-Q water were membrane filtered (cellulose nitrate, 0.2 µm pore diameter, Whatman, Maidstone, Kent, UK), and added to sterile AP1 liquid medium (121°C, 15 min) at room temperature to a final concentration of 1 mM. After autoclaving, the liquid medium was adjusted to pH 5 using 1 M HCl. *Phoma glomerata* grown without Se or Te was used as the control. For solid AP1 media, 15 g L^{-1} Milli-Q water Agar No 1 (Oxoid) was used.

Effect of Se and Te on *Phoma glomerata*

Liquid cultures of *P. glomerata* were harvested after 30 days and the biomass separated by centrifugation at 4000 rpm (4880 g) for 30 min and washed twice with sterile Milli-Q water (autoclaved at 121°C, 15 min). Nanoparticle formation in association with fungal biomass grown with 1 mM Na_2SeO_3 or 1 mM Na_2TeO_3 was examined using scanning electron microscopy (SEM). Fungal pellets grown in the presence of 1 mM Na_2SeO_3 or Na_2TeO_3 for 30 days were cut in half using a sterile scalpel (Swann-Morton, Sheffield, UK) and fixed in 2.5% (v/

v_{aq}) triple-distilled glutaraldehyde in 5 mM 1,4-piperazine *N,N'* bis(2-ethane sulfonic acid) (PIPES) buffer, pH 7.2, for at least 24 h at room temperature. The pH of 5 mM PIPES buffer was adjusted using 1 M NaOH and a Corning pH meter 120 and electrode (Corning Incorporated, Corning, NY, USA). After fixation, samples were rinsed twice in 5 mM PIPES buffer, pH 7.2 (15 min per rinse) and then dehydrated through a graded ethanol series [50%–100% (v/ v_{aq}), 15 min per step]. Samples were then critical point dried using a liquid CO_2 BAL-TEC CPD 0.30 critical point dryer (BAL-TEC company, Canonsburg, PA, USA) and subsequently mounted on aluminium stubs using carbon adhesive tape and stored in a desiccator at room temperature. Prior to electron microscopy, samples were coated with 10 nm Au/Pd using a Cressington 208HR sputter coater (Ted Pella, Redding, CA, USA) and examined using a Philips XL30 environmental scanning electron microscope (ESEM) (Philips XL 30 ESEM FEG) operating at an accelerating voltage of 15 kV.

For confocal microscopy, cultured mycelia in AP1 medium without or supplemented with 1 mM Na_2SeO_3 or Na_2TeO_3 were harvested by centrifugation (13 000 g, 30 min) after 30 days incubation and fixed in 4% paraformaldehyde (PFA) in phosphate buffered saline (PBS) at 4°C overnight, and then permeabilized with 0.5% Triton X-100 in PBS for 30 min prior to the addition of Molecular Probes Hoechst 33342 (nuclear staining dye) (Sigma-Aldrich). The working concentration of Hoechst 33342 was 15 µg mL^{-1} . After 15 min incubation with Hoechst 33342 in the dark, mycelia were washed three times in 0.01 M PBS, pH 7.2 before confocal microscopy. For each sample, 5–10 fields were chosen at random and 0.9-mm thick sections were collected on a laser scanning confocal microscope (Carl Zeiss LSM700; Carl Zeiss Microscopy GmbH, Jena, Germany) using a 40× objective. Maximum intensity projections were made and automatic settings used to locate objects in each image. The offset was set at –65 and objects were filtered using the long axis at <100 µm. Each image was checked manually with at least three replicates.

Characterization of Se and Te nanoparticles

Particles present in the fungal supernatant were harvested by centrifugation at a series of speeds (4 k, 8 k and 13 k × g), each centrifugation step lasting 30 min until the particles in the supernatant were separated from the biomass. Harvested particles were rinsed through a graded ethanol series [50%–100% (v/ v_{aq}), 15 min per step], then rinsed three times with a 20% (w/v) sodium dodecyl sulfate (SDS) solution and finally rinsed three times with autoclaved Milli-Q water (121°C, 15 min) to remove remaining impurities. Particles were subsequently mounted on aluminium scanning electron

microscopy stubs using carbon adhesive tape and stored in a desiccator at room temperature. Nanoparticles separated from the fungal supernatant were examined for elemental composition using energy-dispersive X-ray analysis (EDXA) before Au/Pd coating the samples in order to exclude the Au/Pd peak. A Phoenix EDXA analysis system embedded within the ESEM was used for spectral analysis with an accelerating voltage of 20 kV for at least 100 s.

To further characterize the collected Se- and Te-containing particles, particle size was measured using Fiji software (Schindelin *et al.*, 2012), wherein a user-coded Java ImageJ plugin was employed to evaluate particle-size distribution (PSD) based on the diameter of particles. Approximately, 500 particles were randomly chosen for size measurements. To clarify the PSD, particles were divided into 8–12 groups according to their size range, and their size distribution was fitted according to the Gaussian distribution equation.

X-ray diffraction (XRD) was also employed to characterize the nanoparticles generated by *P. glomerata*. Diffraction patterns were recorded from 3 to 120° 2- θ using Ni-filtered Cu K-alpha radiation, and scanning from 3 to 120° 2- θ , counting for 300 s per step on a Panalytical Xpert Pro diffractometer using a X-celerator position sensitive detector. Mineral phases were identified with reference to patterns in the International Centre for Diffraction Data Powder Diffraction File (PDF).

Fluorescent spectral characteristics of EPS

Excitation emission matrix (EEM) fluorescence spectroscopy was used to assess the involvement of soluble EPS and Se- and Te-bound EPS in the formation of Se and Te NPs. All EEM spectra were measured using a fluorescence spectrophotometer (F-7000; Hitach, Japan) equipped with a 1.0 cm quartz cell and a thermostat bath. EEM spectra were collected from 200 nm to 700 nm in 2 nm increments by varying the excitation wavelength from 200 nm to 500 nm in 5 nm increments. The width of the excitation/emission slit was set at 5.0 nm, and the scanning speed was set to 1200 nm·min⁻¹. The response of the fluorometer to a Milli-Q water blank was subtracted from the fluorescence spectra recorded for samples containing EPS and SeO₃²⁻/TeO₃²⁻ under the same conditions (Song *et al.*, 2012). EEM data were processed using SigmaPlot software, version 12.5 (Systat Software, San Jose, CA, USA).

Fourier-transform infrared spectroscopy and thermogravimetric analysis

To further characterize the elemental Se and Te particles formed by *P. glomerata*, FTIR analysis was used to

identify the functional groups, which could be responsible for stabilizing or determining size and shape. IR spectra of the nanoparticles were recorded using a PerkinElmer Spectrum Two attenuated total reflectance Fourier transform infrared spectrometer (ATR-FTIR) (PerkinElmer, Waltham, MA, USA) equipped with a deuterated tryglycine sulfate (DTGS) detector and consisting of a golden gate single reflection diamond ATR accessory and KBr window. To minimize interferences from the external environment and maintain the consistency of experimental conditions, a background spectrum was recorded before each sample examination. Particles in the fungal supernatant were harvested by centrifugation as described above and after the washing step with Milli-Q water, the aqueous suspension was finally filtered through 0.45 μ m cellulose acetate membrane filters prior to analysis. Aliquots (1 ml) from an aqueous suspension of SeNPs or TeNPs in Milli-Q water was placed on the metal O-ring on the diamond crystal and scanned at a range from 4000 to 450 cm⁻¹, with a resolution of 4 cm⁻¹ and recorded at an average of eight scans at room temperature. Each sample analysis was performed in triplicate.

In order to investigate the thermal degradation characteristics (decomposition temperature, thermal stability, degradation rate and exothermicity) of fungal-formed Se-/Te-containing particles, thermogravimetric analysis (TGA) was employed. The TGA results can elucidate the thermal degradation properties of the nanoparticles and indicate the role of extracellular protein and exopolysaccharide in their stabilization. TGA was performed with a Netzsch STA 409PC TG/DTG/DTA analyser fitted with a SiC furnace (NETZSCH Group, Selb, Germany). Small amounts (4–8 mg) of nanoparticle samples (harvested as described above) were placed in the platinum pan and heated from room temperature to 1000°C at an incremental rate of 10°C per min with dry N₂ as the purge gas at a flow rate of 100 ml min⁻¹. The samples were maintained at 1000°C until they reached constant weight. The results obtained were expressed as a curve of mass loss as a function of temperature.

Sequential extraction and metalloid speciation in Kisgruva sulfide ore

To measure Se and Te content in the Kisgruva sulfide ore samples 450 (Northing/Easting-N59.59360 E009.60893) and 459 (Northing/Easting-N59.59967 E009.60966) (Bullock *et al.*, 2018), sequential extraction and speciation were performed to determine total concentrations of Se and Te species adsorbed onto oxide minerals and organic matter. Speciation and total concentration analysis of the major elements in the Kisgruva sulfide ore samples was performed using an ICP-MS 7900,

coupled to a HPLC 1100 (Agilent Technology, Japan). Concentrations of Se and Te species adsorbed to charged surfaces, such as oxide minerals, were determined by a phosphate buffer extraction method, while the concentrations and speciation of Se and Te adsorbed to organic matter were examined using sodium hydroxide extraction. The Aqua regia residues method was used for total extractable concentrations of Se and Te (Kulp and Pratt, 2004; Di Tullo *et al.*, 2016). For the phosphate buffer extraction method, 0.1 M K_2HPO_4 - KH_2PO_4 buffer at pH 7 was used to desorb ligand-exchangeable Se(IV) and Te (IV) from charged surfaces on oxide minerals or clay particles. For this, 25 ml of phosphate buffer was mixed with 1 g finely ground ore 450 or 459 in 50 ml test tubes and shaken in a shaking incubator at room temperature at 125 rpm for 2 h. After shaking, tubes were centrifuged at 4000 rpm (4880 g) for 30 min at 4 °C, and the supernatants harvested and retained in separate tubes. The remaining ore samples were rinsed with another 10 ml autoclaved (121 °C, 15 min) Milli-Q water, and after shaking and centrifugation, the supernatants were mixed with the previous phosphate buffer extract (Kulp and Pratt, 2004). The sodium hydroxide extraction method was used for extracting tightly bound Se(IV) and Te (IV), and base-soluble inorganic and organic selenides. The ore residues remaining from phosphate buffer extraction were used for the sodium hydroxide extraction. In this method, 25 ml 1 M NaOH was mixed with the ore residues in 50 ml glass tubes and incubated in a water bath at 90 °C for 2 h. After incubation, tubes were cooled and centrifuged at 4000 rpm (4880 g) for 30 min, supernatants being harvested and retained in separate tubes. The remaining ore samples were rinsed with another 10 ml autoclaved (121 °C, 15 min) Milli-Q water, and after shaking and centrifugation, the supernatants were mixed with the previously obtained NaOH extract (Kulp and Pratt, 2004). The residues remaining from the previous sequential-extraction procedures were used to determine total Se and Te using the Aqua regia method [high purity hydrochloric and nitric acids (VWR International Ltd, Poole, UK)] in a heating block within a closed system. Residues were heated until they dissolved and were then tested for total Se and Te content (Kulp and Pratt, 2004; Di Tullo *et al.*, 2016).

Tolerance of P. glomerata to Kisgruva sulfide ore

To investigate effects of the sulfide ores on fungal growth, Kisgruva samples 450 and 459 were ground into powder with a pestle and mortar (Milton Brook, Sturminster Newton, Dorset, UK), and sterilized at 105 °C for 7 days prior to experiments. *Phoma glomerata* was grown in 100 ml AP1 liquid medium with 1 g sulfide ore (samples 450 and 459) in 250-ml Erlenmeyer conical

flasks on an orbital shaking incubator at 125 rpm at 25 °C in the dark for 30 days. Kisgruva sulfide ore samples 450 or 459 were incubated in AP1 medium without *P. glomerata* as a control. Fungal biomass was aseptically harvested after 30 days incubation by centrifugation at 4880 × g for 30 min and washed twice with autoclaved Milli-Q water. The supernatants were further clarified by filtering through 0.45 µm cellulose acetate membrane filters prior to analysis. Growth was evaluated using a tolerance index (TI) calculated as follows: (dry weight of sulfide ore sample exposed mycelium/dry weight of control mycelium). Fungal biomass was oven-dried at 105 °C to constant weight and then ground to a powder using a pestle and mortar. A pH 210 Microprocessor pH Meter (Hanna Instruments, Woonsocket, RI, USA) was used for pH measurements of the culture supernatants. All experiments were conducted at least in triplicate.

Production of extracellular protein and exopolysaccharide by P. glomerata grown with Kisgruva sulfide ore

To examine the effect of sulfide ore on the production of extracellular protein and exopolysaccharide, supernatants harvested after growth of *P. glomerata* in liquid media containing 1 g sulfide ore (sample 450 or 459) for 30 days were centrifuged (12 000 g, 30 min) and the supernatants clarified by filtering through 0.45 µm cellulose acetate membrane filters. After that, the supernatant was purified by dialysis (3500 Da membrane) for 24 h at 4 °C to remove any residual glucose. Extracellular protein was determined using a Bradford protein assay (Bio-Rad Laboratories, Watford, UK) using bovine serum albumin as standard. Polysaccharide content was determined by the phenol-sulfuric acid method using glucose as the standard (Dubois *et al.*, 1956).

XRF spectroscopy for elemental composition of the Kisgruva sulfide ore

Partial elemental composition of the Kisgruva sulfide ore 450 and 459 before and after growth with *P. glomerata* for 30 days at 25 °C was determined by XRF using a Philips PW2424 sequential XRF spectrometer fitted with a RhKa source, and regularly calibrated with certified standard materials. Kisgruva sulfide ore, before and after fungal growth, was harvested after 30 days incubation samples by centrifugation (4880 g, 30 min) and after removal of the supernatant, was washed and resuspended in 50 ml sterile (121 °C, 15 min) Milli-Q water at ambient temperature, and centrifuged again (4880 g, 30 min), this procedure being repeated twice. The ore sample was then dried in an oven at 105 °C for 7 days to constant weight, ground into powder using a

pestle and mortar, and then placed in a Ø27 mm pellet mould and compacted under a load of 75 kN for 5 min and 150 kN for a further 10 min prior to analysis. The results are expressed as oxides.

Laser ablation of Se- or Te-containing Kisgruva sulfide ores after growth of P. glomerata

Sulfide ore samples were cut into blocks, with one surface polished for trace element analysis. X-ray mapping was performed using a New Wave laser ablation system UP213 nm (New Wave Research, Fremont, CA, USA) coupled to an ICP-MS Agilent 7900 (Agilent Technologies, Tokyo, Japan). The laser beam was fired with a spot size of 100 µm, the repetition rate was set at 10 Hz, and at 50 µm s⁻¹ ablation speed with 1 J cm² energy. A 15 s period was applied as a warm-up period before ablation, with a 15 s delay between each ablation. To make sure of restricted oxide formation and maximize the sensitivity, a NIST Glass 612 was used to optimize all the parameters and settings. A reaction cell with 3.0–3.5 ml min⁻¹ hydrogen gas was employed to remove any possible interferences and optimize the Se sensitivity. MASS-1 synthetic polymetal sulfide (US Geological Survey, Reston, VA, USA) and FeS⁻¹ certified reference materials (CRMs) (Slim Group, University of Quebec, Quebec, Canada) were used for quantification.

Speciation and total concentration analysis of Kisgruva sulfide ores after growth of P. glomerata

Speciation and total concentration analysis of the major elements in the Kisgruva sulfide ore samples was performed with an ICP-MS 7900, coupled to a HPLC 1100 (Agilent Technology, Japan). A Hamilton PRP-100 column was used with a mobile phase of 1 ml min⁻¹ (10 mmol L⁻¹, pH 10) phosphate buffer (Sigma-Aldrich). The 100 µl of samples were injected at 4°C with an auto-sampler. Lens parameters were optimized with a solution of 1 µg L⁻¹ of Ga, Y, Tl and Ce, with 3.5 ml min⁻¹ hydrogen used in the reaction cell. The 10 µg L⁻¹ Ge solution was employed as an internal standard to correct any plasma fluctuation and remove any interferences during Se measurement. Isotopes ⁷²Ge, ⁷⁷Se, ⁷⁸Se, ¹²⁵Te and ¹²⁶Te were also monitored. Commercial sodium selenite (Alpha Aesar, Haverhill, MA, USA), sodium selenate (Alpha Aesar), sodium tellurite (Alpha Aesar) and telluric acid (Sigma-Aldrich) were used as standards for total concentration, speciation, external calibration and quantification.

Statistical analysis

All data presented are means of at least three replicates: error bars represent one standard error either side of the mean. SigmaPlot, version 12.5, was used to perform statistical analyses. One-way ANOVA tests on means were performed.

Acknowledgements

G.M.G. gratefully acknowledges research support from Natural Environment Research Council (NE/M010910/1) under the NERC Security of Supply of Mineral Resources Grant Programme: Tellurium and Selenium cycling and supply (TeaSe). G.M.G. also gratefully acknowledges additional support of the Geomicrobiology Group from NERC [NE/M011275/1 (COG³)]. The authors also gratefully acknowledge the help of Dr Yongchang Fan (Materials and Photonics Systems Group, University of Dundee, Dundee, DD1 5EH, Scotland UK) for assistance with scanning electron microscopy, and Dr Alan Prescott and Dr Christopher Lipina (School of Life Sciences, University of Dundee, Dundee, DD1 5EH, Scotland UK) for assistance with confocal microscopy.

Compliance with ethical standards

Ethics approval

This article does not contain any studies with human participants or animals performed by any of the authors.

References

- Aborode, F.A., Raab, A., Foster, S., Lombi, E., Maher, W., Krupp, E.M., and Feldmann, J. (2015) Selenopeptides and elemental selenium in *Thunbergia alata* after exposure to selenite: quantification method for elemental selenium. *Metallomics* **7**: 1056–1066.
- Ahmad, A., Senapati, S., Khan, M.I., Kumar, R., and Sastry, M. (2003) Extracellular biosynthesis of monodisperse gold nanoparticles by a novel extremophilic actinomycete, *Thermomonospora* sp. *Langmuir* **19**: 3550–3553.
- Anjum, F., Bhatti, H.N., Asgher, M., and Shahid, M. (2010) Leaching of metal ions from black shale by organic acids produced by *Aspergillus Niger*. *Appl Clay Sci* **47**: 356–361.
- Armendariz, V., Herrera, I., Peralta-videa, J.R., Joseyacamán, M., Troiani, H., Santiago, P., and Gardea-Torresdey, J.L. (2004) Size controlled gold nanoparticle formation by *Avena sativa* biomass: use of plants in nanobiotechnology. *J Nanopart Res* **6**: 377–382.
- Baesman, S.M., Bullen, T.D., Dewald, J., Zhang, D., Curran, S., Islam, F.S., et al. (2007) Formation of tellurium nanocrystals during anaerobic growth of bacteria that use Te oxyanions as respiratory electron acceptors. *Appl Environ Microbiol* **73**: 2135–2143.
- Bajaj, M., Schmidt, S., and Winter, J. (2012) Formation of Se(0) nanoparticles by *Duganella* sp. and *Agrobacterium*

- sp. isolated from Se-laden soil of north-East Punjab, India. *Microb Cell Fact* **11**: 64.
- Banker, J. (1992) Amide modes and protein conformation. *Biochim Biophys Acta* **1120**: 123–143.
- Birla, S.S., Tiwari, V.V., Gade, A.K., Ingle, A.P., Yadav, A.P., and Rai, M.K. (2009) Fabrication of silver nanoparticles by *Phoma glomerata* and its combined effect against *Escherichia coli*, *Pseudomonas aeruginosa* and *Staphylococcus aureus*. *Lett Appl Microbiol* **48**: 173–179.
- Biswas, S., Dey, R., Mukherjee, S., and Banerjee, P.C. (2013) Bioleaching of nickel and cobalt from lateritic chromite overburden using the culture filtrate of *Aspergillus Niger*. *Appl Biochem Biotechnol* **170**: 1547–1559.
- Bjerkgård, T. (2015) Massive sulfides in Norway. Geological Survey of Norway NGU Focus Nr 2, February 2015.
- Borghese, R., Bruciale, M., Fortunato, G., Lanzi, M., Mezzi, A., Valle, F., et al. (2016) Extracellular production of tellurium nanoparticles by the photosynthetic bacterium *Rhodobacter capsulatus*. *J Hazard Mater* **309**: 202–209.
- Brady, J.M., Tobin, J.M., and Gadd, G.M. (1996) Volatilization of selenite in aqueous medium by a *Penicillium* species. *Mycol Res* **100**: 955–961.
- Bullock, L.A., Perez, M., Armstrong, J.G., Parnell, J., Still, J., and Feldmann, J. (2018) Selenium and tellurium resources in Kistruva Proterozoic volcanogenic massive sulphide deposit (Norway). *Ore Geol Rev* **99**: 411–424.
- Burgstaller, W., and Schinner, F. (1993) Leaching of metals with fungi. *J Biotechnol* **27**: 91–116.
- Cantafio, A.W., Hagen, K.D., Lewis, G.E., Bledsoe, T.L., Nunan, K.M., and Macy, J.M. (1996) Pilot-scale selenium bioremediation of San Joaquin drainage water with *Thauera selenatis*. *Appl Environ Microbiol* **62**: 3298–3303.
- Ceci, A., Kierans, M., Hillier, S., Persiani, A.M., and Gadd, G.M. (2015a) Fungal bioweathering of mimetite and a general geomycological model for lead apatite mineral biotransformations. *Appl Environ Microbiol* **81**: 4955–4964.
- Ceci, A., Rhee, Y.J., Kierans, M., Hillier, S., Pendowski, H., Gray, N., et al. (2015b) Transformation of vanadinite ($\text{Pb}_5(\text{VO}_4)_3\text{Cl}$) by fungi. *Environ Microbiol* **17**: 2018–2034.
- Chasteen, T.G., and Bentley, R. (2003) Biomethylation of selenium and tellurium: microorganisms and plants. *Chem Rev* **103**: 1–26.
- Chen, W., Westerhoff, P., Leenheer, J.A., and Booksh, K. (2003) Fluorescence excitation-emission matrix regional integration to quantify spectra for dissolved organic matter. *Environ Sci Technol* **37**: 5701–5710.
- Debieux, C.M., Dridge, E.J., Mueller, C.M., Splatt, P., Paszkiewicz, K., Knight, I., et al. (2011) A bacterial process for selenium nanosphere assembly. *Proc Nat Acad Sci USA* **108**: 13480–13485.
- Di Tullo, P., Pannier, F., Thiry, Y., Le Hécho, I., and Bueno, M. (2016) Field study of time dependent selenium partitioning in soils using isotopically enriched stable selenite tracer. *Sci Total Environ* **562**: 280–288.
- Dubois, M., Gilles, K.A., Hamilton, J.K., Rebers, P.A., and Smith, F. (1956) Colorimetric method for determination of sugars and related substances. *Anal Chem* **28**: 350–356.
- Espinosa-Ortiz, E.J., Gonzalez-Gil, G., Saikaly, P.E., van Hullebusch, E.D., and Lens, P.N.L. (2015a) Effects of selenium oxyanions on the white-rot fungus *Phanerochaete chrysosporium*. *Appl Microbiol Biotechnol* **99**: 2405–2418.
- Espinosa-Ortiz, E.J., Rene, E.R., van Hullebusch, E.D., and Lens, P.N.L. (2015b) Removal of selenite from wastewater in a *Phanerochaete chrysosporium* pellet based fungal bioreactor. *Int Biodet Biodegrad* **102**: 361–369.
- Espinosa-Ortiz, E.J., Pechaud, Y., Lauchnor, E., Rene, E.R., Gerlach, R., Peyton, B.M., et al. (2016a) Effect of selenite on the morphology and respiratory activity of *Phanerochaete chrysosporium* biofilms. *Bioresour Technol* **210**: 138–145.
- Espinosa-Ortiz, E.J., Rene, E.R., Pakshirajan, K., van Hullebusch, E.D., and Lens, P.N.L. (2016b) Fungal pelleted reactors in wastewater treatment: applications and perspectives. *Chem Eng J* **283**: 553–571.
- Espinosa-Ortiz, E.J., Shakya, M., Jain, R., Rene, E.R., van Hullebusch, E.D., and Lens, P.N.L. (2016c) Sorption of zinc onto elemental selenium nanoparticles immobilized in *Phanerochaete chrysosporium* pellets. *Environ Sci Pollut Res Int* **23**: 21619–21630.
- Espinosa-Ortiz, E.J., Rene, E.R., Guyot, F., van Hullebusch, E.D., and Lens, P.N.L. (2017) Biomineralization of tellurium and selenium-tellurium nanoparticles by the white-rot fungus *Phanerochaete chrysosporium*. *Int Biodet Biodegrad* **124**: 258–266.
- Eswayah, A.S., Smith, T.J., and Gardiner, P.H. (2016) Microbial transformations of selenium species of relevance to bioremediation. *Appl Environ Microbiol* **82**: 4848–4859.
- Gadd, G.M. (1993) Microbial formation and transformation of organometallic and organometalloid compounds. *FEMS Microbiol Rev* **11**: 297–316.
- Gadd, G.M. (2007) Geomycology: biogeochemical transformations of rocks, minerals, metals and radionuclides by fungi, bioweathering and bioremediation. *Mycol Res* **111**: 3–49.
- Gadd, G.M. (2010) Metals, minerals and microbes: geomicrobiology and bioremediation. *Microbiol* **156**: 609–643.
- Gade, A.K., Gaikwad, S.C., Duran, N., and Rai, M.K. (2014) Green synthesis of silver nanoparticles by *Phoma glomerata*. *Micron* **59**: 52–59.
- Gharieb, M.M., and Gadd, G.M. (1998) Evidence for the involvement of vacuolar activity in metal(loid) tolerance: vacuolar-lacking and -defective mutants of *Saccharomyces cerevisiae* display higher sensitivity to chromate, tellurite and selenite. *Biometals* **11**: 101–106.
- Gharieb, M.M., and Gadd, G.M. (2004) Role of glutathione in detoxification of metal(loid)s by *Saccharomyces cerevisiae*. *Biometals* **17**: 183–188.
- Gharieb, M.M., Kierans, M., and Gadd, G.M. (1999) Transformation and tolerance of tellurite by filamentous fungi: accumulation, reduction, and volatilization. *Mycol Res* **103**: 299–305.
- Gudadhe, J.A., Bonde, S.R., Gaikwad, S.C., Gade, A.K., and Rai, M.K. (2011) *Phoma glomerata*: a novel agent for fabrication of iron oxide nanoparticles. *J Bionanosci* **5**: 138–142.
- Guo, Y., Pan, D., Li, H., Sun, Y., Zeng, X., and Yan, B. (2013) Antioxidant and immunomodulatory activity of selenium exopolysaccharide produced by *Lactococcus lactis* subsp. *Lactis*. *Food Chem* **138**: 84–89.

- Jacob, J.M., Lens, P.N.L., and Balakrishnan, R.M. (2016) Microbial synthesis of chalcogenide semiconductor nanoparticles: a review. *J Microbial Biotechnol* **9**: 11–21.
- Jain, R., Jordan, N., Weiss, S., Foerstendorf, H., Heim, K., Kacker, R., *et al.* (2015) Extracellular polymeric substances govern the surface charge of biogenic elemental selenium nanoparticles. *Environ Sci Technol* **49**: 1713–1720.
- Jiang, S., Ho, C.T., Lee, J.H., van Duong, H., Han, S., and Hur, H.G. (2012) Mercury capture into biogenic amorphous selenium nanospheres produced by mercury resistant *Shewanella putrefaciens* 200. *Chemosphere* **87**: 621–624.
- Johnson, D.B. (2014) Biomining – biotechnologies for extracting and recovering metals from ores and waste materials. *Curr Opin Biotechnol* **30**: 24–31.
- Johnson, D.B., Grail, B.M., and Hallberg, K.B. (2013) A new direction for biomining: extraction of metals by reductive dissolution of oxidized ores. *Minerals* **3**: 49–58.
- Kim, Y.H., Lee, H.S., Kwon, H.J., Patnaik, B.B., Nam, K.W., Han, Y.S., *et al.* (2014) Effects of different selenium levels on growth and regulation of laccase and versatile peroxidase in white-rot fungus, *Pleurotus eryngii*. *World J Microbial Biotechnol* **30**: 2101–2109.
- Kirtzel, J., Ueberschaar, N., Deckert-Gaudig, T., Krause, K., Deckert, V., Gadd, G.M., and Kothe, E. (2020) Organic acids, siderophores, enzymes, and mechanical pressure for black slate bioweathering with the basidiomycete *Schizophyllum commune*. *Environ Microbiol* **22**: 1535–1546.
- Kong, J., and Yu, S. (2007) Fourier transform infrared spectroscopic analysis of protein secondary structures. *Acta Biochem Biophys Sinica* **39**: 549–559.
- Kotková, J., Kullerud, K., Šrein, V., Drábek, M., and Škoda, R. (2018) The Kongsberg silver deposits, Norway: Ag-Hg-Sb mineralization and constraints for the formation of the deposits. *Miner Deposita* **53**: 531–545.
- Krimm, S., and Bandekar, J. (1986) Vibrational spectroscopy and conformation of peptides, polypeptides, and proteins. *Adv Protein Chem* **38**: 181–364.
- Kulp, T.R., and Pratt, L.M. (2004) Speciation and weathering of selenium in upper cretaceous chalk and shale from South Dakota and Wyoming, USA. *Geochim Cosmochim Acta* **68**: 3687–3701.
- Lawson, S., and Macy, J. (1995) Bioremediation of selenium in oil refinery wastewater. *Appl Microbiol Biotechnol* **43**: 762–765.
- Li, D.B., Cheng, Y.Y., Wu, C., Li, W.W., Li, N., Yang, Z.C., *et al.* (2014) Selenite reduction by *Shewanella oneidensis* MR-1 is mediated by fumarate reductase in periplasm. *Sci Rep* **4**: 3735.
- Li, Q., and Gadd, G.M. (2017) Biosynthesis of copper carbonate nanoparticles by ureolytic fungi. *Appl Microbiol Biotechnol* **101**: 7397–7407.
- Liang, X., and Gadd, G.M. (2017) Metal and metalloid biorecovery using fungi. *J Microbial Biotechnol* **10**: 1199–1205.
- Liang, X., Perez, M.A.M.-J., Nwoko, K.C., Egbers, P., Feldmann, J., Csetenyi, L., and Gadd, G.M. (2019) Fungal formation of selenium and tellurium nanoparticles. *Appl Microbiol Biotechnol* **103**: 7241–7259.
- Liu, F., Csetenyi, L., and Gadd, G.M. (2019) Amino acid secretion influences the size and composition of copper carbonate nanoparticles synthesized by ureolytic fungi. *Appl Microbiol Biotechnol* **103**: 7217–7230.
- Mal, J., Nanchaiah, Y.V., Maheshwari, N., van Hullebusch, E.D., and Lens, P.N.L. (2017) Continuous removal and recovery of tellurium in an upflow anaerobic granular sludge bed reactor. *J Hazard Mater* **327**: 79–88.
- Mandal, D., Bolander, M.E., Mukhopadhyay, D., Sarkar, G., and Mukherjee, P. (2006) The use of microorganisms for the formation of metal nanoparticles and their application. *Appl Microbiol Biotechnol* **69**: 485–492.
- Mehta, K.D., Das, C., and Pandey, B.D. (2010) Leaching of copper, nickel and cobalt from Indian Ocean manganese nodules by *Aspergillus Niger*. *Hydrometallurgy* **105**: 89–95.
- Munoz, A.H.S., Kubacka, K., Wrobel, K., Corona, J.F.G., Yathavakilla, S.K.V., Caruso, J.A., and Wrobel, K. (2006) Se-enriched mycelia of *Pleurotus ostreatus*: distribution of selenium in cell walls and cell membranes/cytosol. *J Agric Food Chem* **54**: 3440–3444.
- Nanchaiah, Y.V., Venkata Mohan, S., and Lens, P.N.L. (2016) Biological and bioelectrochemical recovery of critical and scarce metals. *Trends Biotechnol* **34**: 137–155.
- Oremland, R.S., Herbel, M.J., Blum, J.S., Langley, S., Beveridge, T.J., Ajayan, P.M., *et al.* (2004) Structural and spectral features of selenium nanospheres produced by Se-respiring bacteria. *Appl Environ Microbiol* **70**: 52–60.
- Piacenza, E., Presentato, A., and Turner, R.J. (2018a) Stability of biogenic metal(loid) nanomaterials related to the colloidal stabilization theory of chemical nanostructures. *Crit Rev Biotechnol* **38**: 1137–1156.
- Piacenza, E., Presentato, A., Zonaro, E., Lampis, S., Vallini, G., and Turner, R.J. (2018b) Microbial-based bioremediation of selenium and tellurium compounds. In *Bio-sorption*, Vol. **2018**, Derco, J., and Vrana, B. (eds). London, UK: IntechOpen, pp. 117–147.
- Rosenfeld, C.E., Kenyon, J.A., James, B.R., and Santelli, C. M. (2017) Selenium (IV,VI) reduction and tolerance by fungi in an oxic environment. *Geobiology* **15**: 441–452.
- Sarkar, J., Dey, P., Saha, S., and Acharya, K. (2011) Mycosynthesis of selenium nanoparticles. *Micro Nano Lett* **6**: 599–602.
- Schindelin, J., Arganda-Carreras, I., Frise, E., Kaynig, V., Longair, M., Pietzsch, T., *et al.* (2012) Fiji: an open-source platform for biological-image analysis. *Nat Methods* **9**: 676–682.
- Schippers, A., Hedrich, S., Vasters, J., Drobe, M., Sand, W., and Willscher, S. (2013) Biomining: metal recovery from ores with microorganisms. In *Geobiotechnology I. Advances in Biochemical Engineering/Biotechnology*, Vol. **141**, Schippers, A., Glombitza, F., and Sand, W. (eds). Berlin, Heidelberg: Springer, pp. 1–47.
- Sharma, G., Sharma, A.R., Bhavesh, R., Park, J., Ganbold, B., Nam, J.S., and Lee, S.S. (2014) Biomolecule-mediated synthesis of selenium nanoparticles using dried *Vitis vinifera* (Raisin) extract. *Molecules* **19**: 2761–2770.
- Soda, S., Takahashi, H., Kagami, T., Miyake, M., Notaguchi, E., Sei, K., *et al.* (2012) Biotreatment of selenium refinery wastewater using pilot-scale granular sludge

- and swim-bed bioreactors augmented with a selenium-reducing bacterium *Pseudomonas stutzeri* NT-I. *Jpn J Water Treat Biol* **48**: 63–71.
- Song, W., Pan, X., and Zhang, D. (2012) Lead complexation of soluble and bound extracellular polymeric substances from activated sludge: characterized with fluorescence spectroscopy and FTIR spectroscopy. *Biotechnol Bio-technol Equip* **26**: 3371–3377.
- Sonkusre, P., Nanduri, R., Gupta, P., and Cameotra, S.S. (2014) Improved extraction of intracellular biogenic selenium nanoparticles and their specificity for cancer chemoprevention. *J Nanomed Nanotechnol* **5**: 194.
- Sweeney, R.Y., Mao, C., Gao, X., Burt, J.L., Belcher, A.M., Georgiou, G., and Iverson, B.L. (2004) Bacterial biosynthesis of cadmium sulfide nanocrystals. *Chem Biol* **11**: 1553–1559.
- Tugarova, A.V., Mamchenkova, P.V., Dyatlova, Y.A., and Kamnev, A.A. (2017) FTIR and Raman spectroscopic studies of selenium nanoparticles synthesised by the bacterium *Azospirillum thiophilum*. *Spectrochim Acta A Mol Biomol Spectrosc* **192**: 458–463.
- Vetchinkina, E., Loshchinina, E., Kursky, V., and Nikitina, V. (2013) Reduction of organic and inorganic selenium compounds by the edible medicinal basidiomycete *Lentinula edodes* and the accumulation of elemental selenium nanoparticles in its mycelium. *J Microbiol* **51**: 829–835.
- Wei, Z., Kierans, M., and Gadd, G.M. (2012a) A model sheet mineral system to study fungal bioweathering of mica. *Geomicrobiol J* **29**: 323–331.
- Wei, Z., Hillier, S., and Gadd, G.M. (2012b) Biotransformation of manganese oxides by fungi: solubilization and production of manganese oxalate biominerals. *Environ Microbiol* **14**: 1744–1753.
- Wei, Z., Liang, X., Pendrowski, H., Hillier, S., Suntornvongsagul, K., Sihanonth, P., and Gadd, G.M. (2013) Fungal biotransformation of zinc silicate and sulphide mineral ores. *Environ Microbiol* **15**: 2173–2186.
- Yang, Y., Ferrier, J., Csetenyi, L., and Gadd, G.M. (2019) Direct and indirect bioleaching of cobalt from low grade laterite and pyritic ores by *Aspergillus Niger*. *Geomicrobiol J* **36**: 940–949.
- Yang, Y., Song, W., Ferrier, J., Liu, F., Csetenyi, L., and Gadd, G.M. (2020) Biorecovery of cobalt and nickel using biomass-free culture supernatants from *Aspergillus Niger*. *Appl Microbiol Biotechnol* **104**: 417–425.
- Zhang, L., Li, D., and Gao, P. (2012) Expulsion of selenium/protein nanoparticles through vesicle-like structures by *Saccharomyces cerevisiae* under microaerophilic environment. *World J Microbiol Biotechnol* **28**: 3381–3386.
- Zhu, Z.Y., Liu, F., Gao, H., Sun, H., Meng, M., and Zhang, Y. M. (2016) Synthesis, characterization and antioxidant activity of selenium polysaccharide from *Cordyceps militaris*. *Int J Biol Macromol* **93**: 1090–1099.